EXPERIMENTAL AND THEORETICAL INVESTIGATIONS ON THE CASSINI RPWS ANTENNAS

H. O. Rucker*, W. Macher*, and S. Albrecht†

Abstract

The Radio and Plasma Wave Science experiment (RPWS) aboard the Cassini spacecraft is designed to primarily observe the Saturnian radio emission. Using three independent monopoles the RPWS experiment is capable of providing data for direction finding of incoming radio waves, which mainly consists of the determination of the four Stokes parameters. For this procedure it is of fundamental importance to exactly know the effective antenna length vectors which, due to the influence of the metallic spacecraft body, significantly deviate from the direction of the physical antenna rods. On the one side, rheometry measurements with a down-scaled spacecraft model immersed in a homogeneous electric field within a water-filled tank, have enabled the experimental determination of the direction of the effective antenna length vectors (the effective antenna axes) as well as their magnitudes. On the other side, theoretical investigations have been performed by numerically simulating the spacecraft-antenna system as a simplified wire grid model, the antennas being excited with a frequency of 500 kHz in the middle of the frequency range of interest. Corresponding results, both from the experimental and theoretical point of view, are discussed.

1 Introduction

The Radio and Plasma Wave Science (RPWS) experiment on the Cassini spacecraft is devised for the reception of radio and plasma waves, specifically from the Saturnian Kilometric Radiation (SKR), by three linear monopole antennas. These antennas are electrically short compared with the SKR wavelength, which enables the description of the reception properties of the antenna system by means of the effective length vector $\mathbf{h}_{\text{eff}}$. For a stand-alone dipole $\mathbf{h}_{\text{eff}}$ is parallel to the mechanical dipole axis, wheras in the presence of perturbing scatterers, e.g. a spacecraft body, $\mathbf{h}_{\text{eff}}$ will be displaced from the mechanical axis. For direction finding measurements, i.e. the determination of the direction of arrival

*Space Research Institute, Austrian Academy of Sciences, 8010 Graz, AUSTRIA
†Institute for High Frequency Technique, Ruhr-University Bochum, 44780 Bochum, FRG

and polarization of incident waves, it is of prime importance to exactly know the antenna system characteristics defined by $\mathbf{h}_{\text{eff}}$. Therefore the determination of the displacement that $\mathbf{h}_{\text{eff}}$ undergoes from the corresponding mechanical element is the focal point of the present paper.

Considering short antennas means that the dimension D of the whole antenna system is much smaller than the wavelength λ of the received electromagnetic wave. In this case the relation between the electric field vector $\mathbf{E}$ of the electromagnetic wave and the voltage V excited at the open antenna feed terminals is completed by the so-called effective antenna length vector $\mathbf{h}_{\text{eff}}$, which is constant (independent of frequency and direction of incoming wave), to give

$$V = \mathbf{E} \cdot \mathbf{h}_{\text{eff}}. \tag{1}$$

Since this holds in the limit $\lambda \to \infty$, it is possible to utilize the electrostatic analogy for the determination of $\mathbf{h}_{\text{eff}}$. In order to distinguish methods that are not based on the electrostatic analogy, they will be called high frequency methods. Beside the classification by frequency the methods can be devided into experimental and theoretical ones. As shown in Table 1, four classes of methods are so defined for the determination of $\mathbf{h}_{\text{eff}}$. In the present paper the method of rheometry, a quasi-static method for short antennas, and the application of a numerical code, ASAP, based on the electric field integral equation, are described and applied to the Cassini RPWS antenna system.

Table 1: Methods for the determination of effective length vectors of short antennas, classified by frequency and way of implementation.

	Experimental	**Theoretical**
High-frequency	Measurements with scale model serving as receiver[1]	Numerical codes based on EFIE and MFIE (electric and magnetic field integral equation)
Quasi-static	Rheometry: Electrolytic tank measurements with scale model[2]	Electrostatic potential analogy

[1] Performed for the Voyager PRA antennas by Riddle, [1976].
[2] Performed for the Cassini RPWS antennas by Rucker et al., [1996].

2 Rheometry measurements

Rheometry takes advantage of the equivalence of the field solutions in the real wave receiving situation and under the conditions of the rheometry experiment, where a homogeneous quasi-static electric field is generated within an electrolytic medium, thereby simulating an electromagnetic plane wave incident to the antenna system. A detailed description of rheometry principles is given by Rucker et al. [1996] (previously within different contexts Hoang [1972], Hulin and Epstein [1973]). So the rheometry experiment essentially measures the reaction of the antenna system on the electric field, thereby applying different

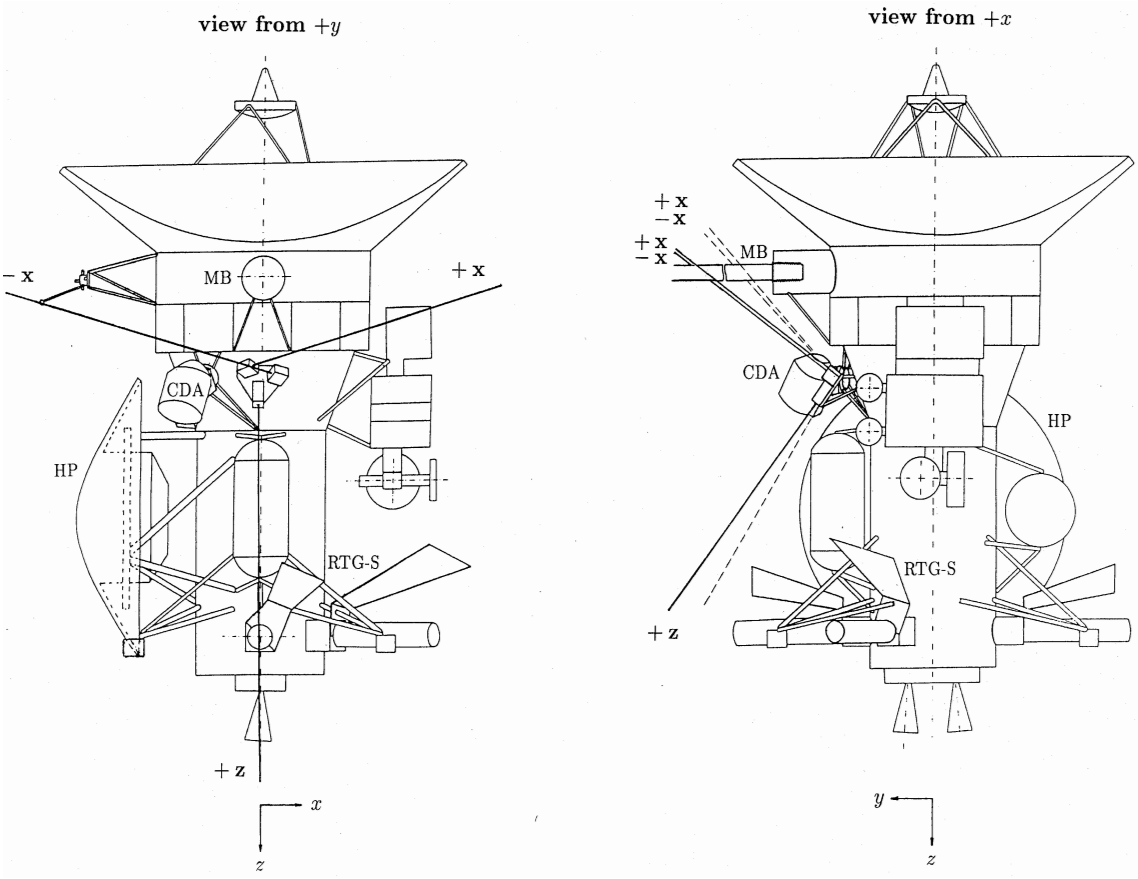

Figure 1: Drawings of the Cassini spacecraft model in elevation. Abbreviations are magnetometer boom MB, cosmic dust analyzer CDA, Huygens probe HP, shades of the radioisotope thermoelectric generators RTG-S. Mechanical antenna elements are drawn as solid lines, the corresponding effective antenna axes as dashed lines. (After Rucker et al., [1996].)

positions of the spacecraft-antenna system relative to the electric field in order to resolve the effective antenna axes.

The Cassini rheometry model schematics on scale 1:30, derived from a JPL released spacecraft configuration, show a cylindrical main body with the high gain antenna and attached structures (Figure 1 and color plate, Figure 3). Most important with regard to the reception properties of the RPWS antennas are the Huygens Probe (HP), the Magnetometer Boom (MB), the Cosmic Dust Analyser (CDA), the experimental platform on the opposite side of the HP, the Radioisotope Thermoelectric Generators (RTGs) with shades (RTG-S), and some tanks. The spacecraft-fixed coordinate system is defined as shown in Figure 1, with the colatitude ϑ and azimuth φ as spherical coordinates with respect to this reference frame. The antenna elements are named after their respective main directions, $+\mathbf{x}$, $-\mathbf{x}$, and $+\mathbf{z}$.

The rheometry experimental setup (Figure 2) comprises an electrolytic tank (with non-conducting walls made of marble) of size $(2 \times 1 \times 1)\,\mathrm{m}$, filled with tap water. Steel plates build a capacitor which is driven by an alternating voltage of about 0.4 Volts rms and 1.03 kHz (alternating current is used to avoid polarization effects), maintaining

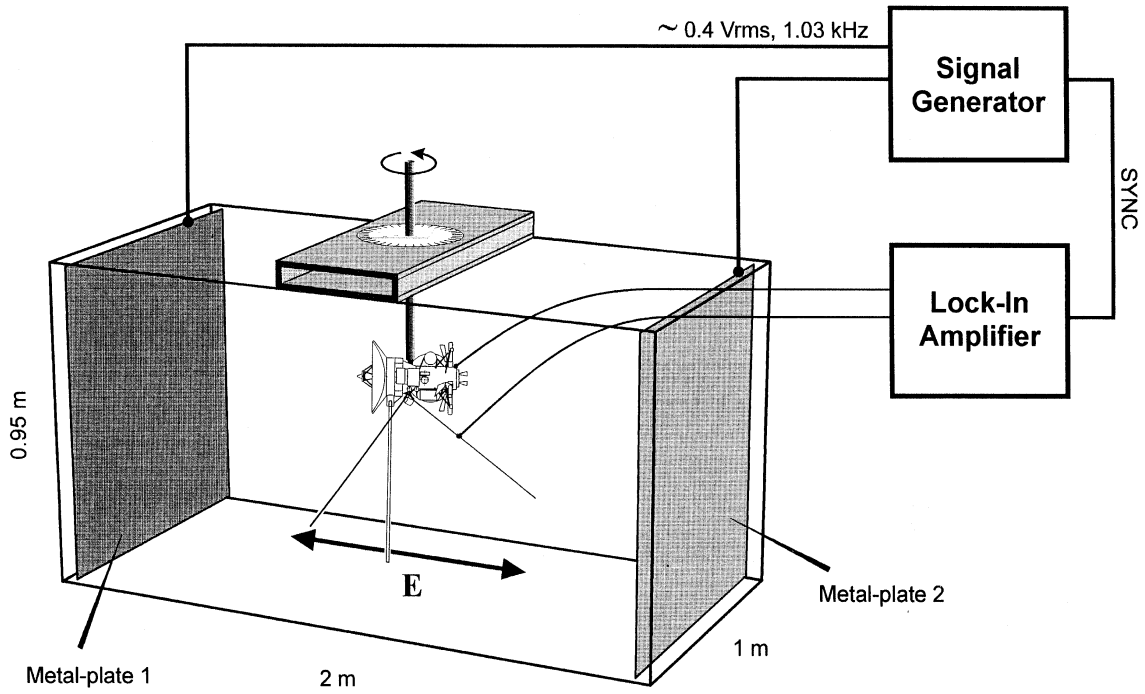

Figure 2: Scheme of the experimental set-up for the rheometry measurements (after Rucker et al., [1996]).

a homogeneous quasi-static electric field within the tank. The down-scaled spacecraft model is then immersed into this electric field. The voltage induced at the open terminals of the receiving antenna is given by Eq. (1). In order to determine $\mathbf{h}_{\text{eff}}$ of one antenna the model is turned around the suspension axis into the position where the voltage response measured by a lock-in amplifier at the antenna vanishes. From the zero response positions obtained for three orthogonal suspensions of the model the position of the effective antenna axis in the spacecraft-fixed reference frame can be determined.

A number of rheometry test series have been performed, the results of which are summarized in Table 2, giving the magnitude $h = |\mathbf{h}_{\text{eff}}|$ and direction (ϑ, φ) of $\mathbf{h}_{\text{eff}}$ for 5 antenna configurations (for the dipole $+\mathbf{x}$ and $-\mathbf{x}$ are driven versus each other and the spacecraft body serves as independent parasitic body, for the common mode $+\mathbf{x}$ and $-\mathbf{x}$ are short-circuited and driven versus the spacecraft body). In section 4 these results will be compared with those found by numerical computer simulations. In Figure 1 the mechanical antenna elements ($+\mathbf{x}$, $-\mathbf{x}$, and $+\mathbf{z}$) are depicted as solid lines, their effective antenna axes as dashed lines, respectively. As can be seen in the view from $+x$, the projections on the yz-plane of the mechanical elements and the corresponding effective axes significantly deviate from each other, whereas the respective projections onto the xz-

Figure 3: (plate, next page) Pictures of the Cassini rheometry scale model (scale 1:30), with and without Huygens probe. The model is made of brass and gold-plated (as are the antennas) to minimize resistance and reactions with the water during the measurements.

Table 2: Effective length vectors of the RPWS antennas on board the Cassini spacecraft as found by rheometry measurements.

Antenna	Physical			$\mathbf{h}_{\text{eff}}$ – HP on			$\mathbf{h}_{\text{eff}}$ – HP off		
	h	ϑ	φ	h	ϑ	φ	h	ϑ	φ
$+\mathbf{z}$	5.0	37.0	90.0	4.4	31.4	91.2	4.4	30.8	92.9
$+\mathbf{x}$	5.0	107.5	24.8	4.0	107.9	16.5	4.0	107.6	16.3
$-\mathbf{x}$	5.0	107.5	155.2	4.0	107.3	162.7	4.0	106.4	163.5
Dipole	8.7	90.0	0.0	7.3	90.5	359.8	7.4	90.6	359.9
Common	2.5	127.0	90.0	1.6	137.9	88.6	1.6	137.9	91.0

The results relate to two different configurations, defined by whether the Huygens probe (HP) is mounted or taken off. The given values represent spherical coordinates in the spacecraft-fixed reference frame (see Figure 1), with colatitude ϑ and azimuth φ in degrees and magnitude $h = |\mathbf{h}_{\text{eff}}|$ in meters. The column headed "physical" contains the corresponding effective length vectors for the imaginary case of an infinitely small spacecraft body, whereby the angular values for $+\mathbf{z}$, $+\mathbf{x}$ and $-\mathbf{x}$ represent the direction of the mechanical antenna elements. (After Rucker et al., [1996]).

plane nearly coincide, so only the mechanical elements are indicated in the view from $+y$. An interpretation of the rheometry results and their accuracy can be found in Rucker et al., [1996], including a comparison with the antennas of the Planetary Radio Astronomy (PRA) experiment on board the Voyager spacecraft.

3 Numerical simulation

3.1 Description of the method

As the electromagnetic field is readily obtained from the current distribution $\mathbf{J}$, the central task of scattering and transmission problems is the calculation of the surface currents on the involved conducting bodies. The boundary value problems describing this situation lead to the electric and magnetic field integral equation (EFIE, MFIE). For the solution of these equations, the method of moments is applied [Harrington, 1985]. Thereby the current distribution is represented by suitable basis functions and the equations are approximately fulfilled by actually solving their scalar product with special test (or weighting) functions. The various numerical codes that implement the moment method differ mainly in the kind of grid-modelling of the sample and how they choose and handle basis and test functions.

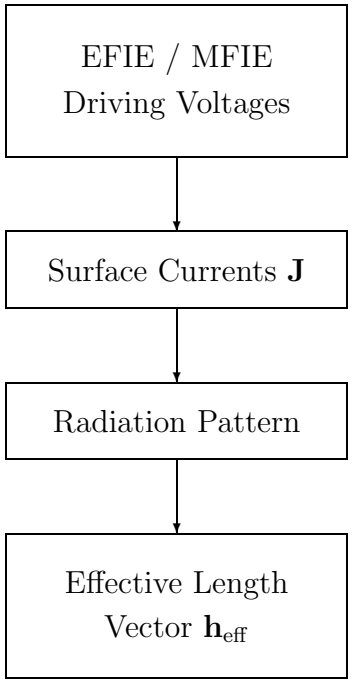

With the programs NEC (Numerical Electromagnetic Code) and ASAP (Antennas Scattering Analysis Program) numerical simulations have been performed for the Cassini RPWS antennas at a frequency of 500 kHz, i.e $\lambda = 600$ meters – about 100 times the dimension D of the spacecraft. NEC uses piecewise sinusoidal subdomain functions as basis functions, whereas ASAP uses linear ones. Therefore ASAP yields more reliable results than NEC as the wavelength is much greater than the dimension of the antenna system. ASAP uses wire grid modelling, reducing the problem to a matrix equation of integrals involving the Green's function and the model grid geometry. The inversion of the equation applied to the driving electric fields/voltages yields the current distribution on the wire grid, from which the radiation pattern and further the effective antenna length vector can be obtained.

First the vector potential $\mathbf{A}$ can be calculated from the current distribution $I(\mathbf{r}')$ on the grid by (harmonic time dependence with circular frequency $\omega = kc$)

$$\mathbf{A}(\mathbf{r}) = \frac{\mu_0}{4\pi} \int I(\mathbf{r}') \frac{e^{ik|\mathbf{r}-\mathbf{r}'|}}{|\mathbf{r}-\mathbf{r}'|} \mathrm{d}\mathbf{s}', \tag{2}$$

from which $\mathbf{E}$ and $\mathbf{B}$ are obtained by

$$\mathbf{B} = \mathrm{rot}\, \mathbf{A}, \tag{3}$$

$$\mathbf{E} = \frac{ic^2}{\omega} \mathrm{rot}\, \mathbf{B}. \tag{4}$$

In the far zone the fields take on the asymptotic form

$$\mathbf{A} = \frac{e^{ikr}}{r} \int I(\mathbf{r}') e^{-ik\mathbf{e}_r \cdot \mathbf{r}'} \mathrm{d}\mathbf{s}', \tag{5}$$

$$\mathbf{B} = ik\, \mathbf{e}_r \times \mathbf{A}, \tag{6}$$

$$\mathbf{E} = -i\omega\, \mathbf{e}_r \times (\mathbf{e}_r \times \mathbf{A}), \tag{7}$$

where

$$\mathbf{e}_r = \frac{\mathbf{r}}{r}, \quad r = |\mathbf{r}|. \tag{8}$$

The integral is to be taken over all line elements of the spacecraft grid. The radiation power into the solid angle $\mathrm{d}\Omega$ is then given by ($\mathbf{B}^*$ complex conjugate of $\mathbf{B}$)

$$\mathrm{d}P = r^2 \mathrm{d}\Omega\, \mathbf{e}_r \cdot \frac{1}{2} (\mathbf{E} \times \mathbf{B}^*/\mu_0), \tag{9}$$

$$\frac{\mathrm{d}P}{\mathrm{d}\Omega} = \frac{\omega^2}{2\mu_0 c} |\mathbf{r} \times \mathbf{A}|^2. \tag{10}$$

The effective antenna axis is eventually found as the direction of minimum radiated power.

3.2 Grid-design for the Cassini spacecraft

The modelling of the surface grid is performed in two steps. Design 1 is limited to the outline of the spacecraft main body, whereby in design 2 the magnetometer boom

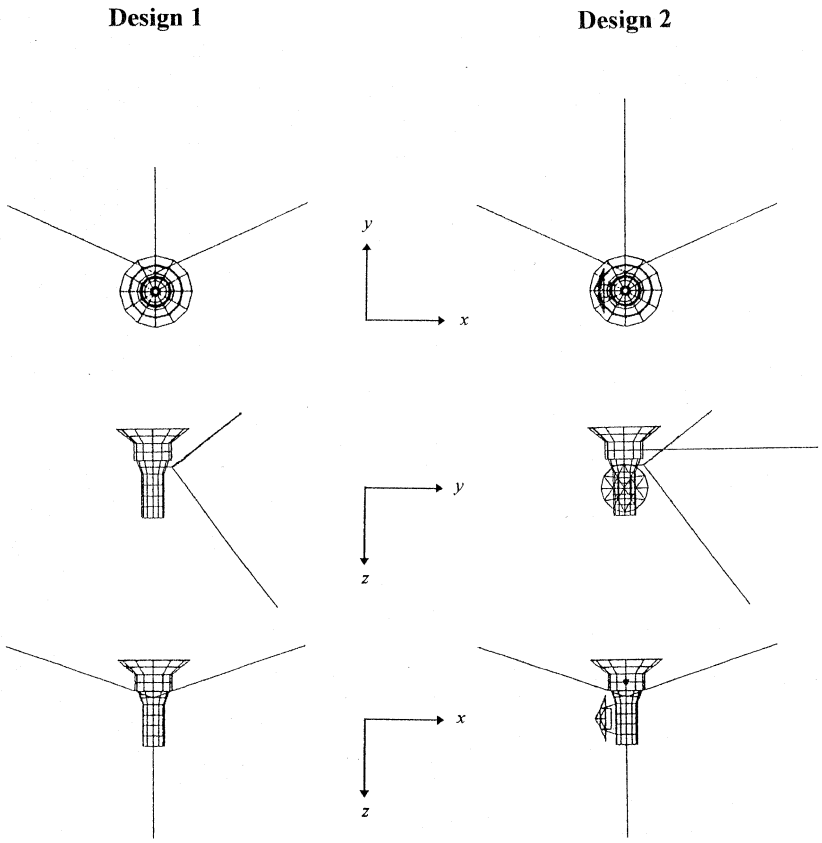

Figure 4: Grid models for the Cassini spacecraft as used for the numerical simulations of the RPWS antenna system.

(MB) and the Huygens probe (HP) are added (Figure 4). For design 2 all numerical simulations are additionally made for removed HP, but leaving the HP-adapter attached to the spacecraft body (some grid elements simulating the region of the HP-attachement). These measurements are important for comparison, as the adapter will remain on the spacecraft after the HP will have been jettisoned towards Titan.

There are a number of features that are not included in the grid-modelling, having probably significant influence on the reception properties of the antennas. The most important ones are (compare Figure 1) the experimental platform, the RTGs with their shades, and some tanks (the CDA showed not such a great influence in the rheometry measurements as previously expected). To add these parts in a further developed design 3 grid is left open for future simulations. This will ensure best comparability with rheometry results.

3.3 Results of ASAP simulations

The results given below are calculated with ASAP for a frequency of 500 kHz. Investigations based on other frequencies were performed to study the due variation of effective length vectors. The results proved ASAP very consistent down to 300 kHz for our problem, getting more and more instable for lower frequencies.

All calculations are performed for seven different modes, which define special antenna-spacecraft circuit configurations as can be seen in Table 3. The ON-antenna elements are held at 10 Volts versus spacecraft, whereas the OFF-antennas are short-circuited to the spacecraft body (ground). Two or three ON-antennas for the same mode are driven in phase, i.e. there is no phase difference between their respective feed points. For the monopoles there is only one antenna element, respectively, that does not lie at the same potential as the spacecraft body (modes 3, 4 and 5). These are the ones that are important for direction finding techniques. Table 3 contains the effective antenna axes found for design 1 and 2. We can see that the monopoles show great differences between the two designs in terms of azimuth φ. This behaviour could be expected for the non-symmetric position of the Huygens probe with regard to the plane spanned by the respective antenna element and the spacecraft axis (z-axis). Concerning the two variants of design 2, we can also recognize a significant bending of the $\mathbf{h}_{\text{eff}}$-direction of the $+\mathbf{z}$-antenna by taking off the Huygens probe. This confirms the rheometry results.

Table 3: Effective antenna axes as found by ASAP simulations for grid design 1 and 2, and for seven modes of excitation (explanation in text).

	Antennas			Design 1		Design 2			
						HP on		HP off	
Mode	$+\mathbf{x}$	$-\mathbf{x}$	$+\mathbf{z}$	ϑ	φ	ϑ	φ	ϑ	φ
1	ON	OFF	ON	66.0	46.5	63.0	36.5	62.0	36.5
2	OFF	ON	ON	66.0	133.5	63.0	135.0	61.5	139.0
3($+\mathbf{x}$)	ON	OFF	OFF	106.0	22.5	106.5	14.5	104.5	14.5
4($-\mathbf{x}$)	OFF	ON	OFF	106.0	157.5	106.5	161.0	106.0	162.0
5($+\mathbf{z}$)	OFF	OFF	ON	34.5	90.0	29.0	83.5	28.0	85.0
6	ON	ON	OFF	126.0	90.0	136.5	83.5	135.5	85.5
7	ON	ON	ON	76.0	90.0	72.5	84.5	70.0	86.5

ϑ and φ are colatitude and azimuth in the spacecraft fixed reference frame, all angular values in degrees. For the monopole modes 3 through 5 the corresponding names are given.

The antenna input impedances calculated by ASAP are practically imaginary (real part is negligible) for all modes, lying between 4.5 and 7.0 kOhms in magnitude, corresponding to capacitances between 70 and 45 pF. For the monopole modes we get 67 pF, which is smaller than the values found by rheometry of about 105 pF. The discrepancy is mainly due to differences in the modelling of the antennas feed zone. In particular the distance between the spacecraft and the end points of the antenna rods is about 30 cm in the ASAP grid model, which is too large for a realistic representation. But this choice of distance was necessary for the ASAP algorithm to work reliably.

To illustrate the results of the numerical ASAP calculation the planar radiation patterns for the $+\mathbf{z}$-antenna (excitation mode 5) are shown beside a depiction of the wire grid model (Figure 5). The depicted 2-dimensional radiation patterns are obtained by intersection of the 3-dimensional radiation pattern with the xy-, xz- and yz-plane of the spacecraft fixed reference frame, respectively. The shown grid drawing is the projection of the

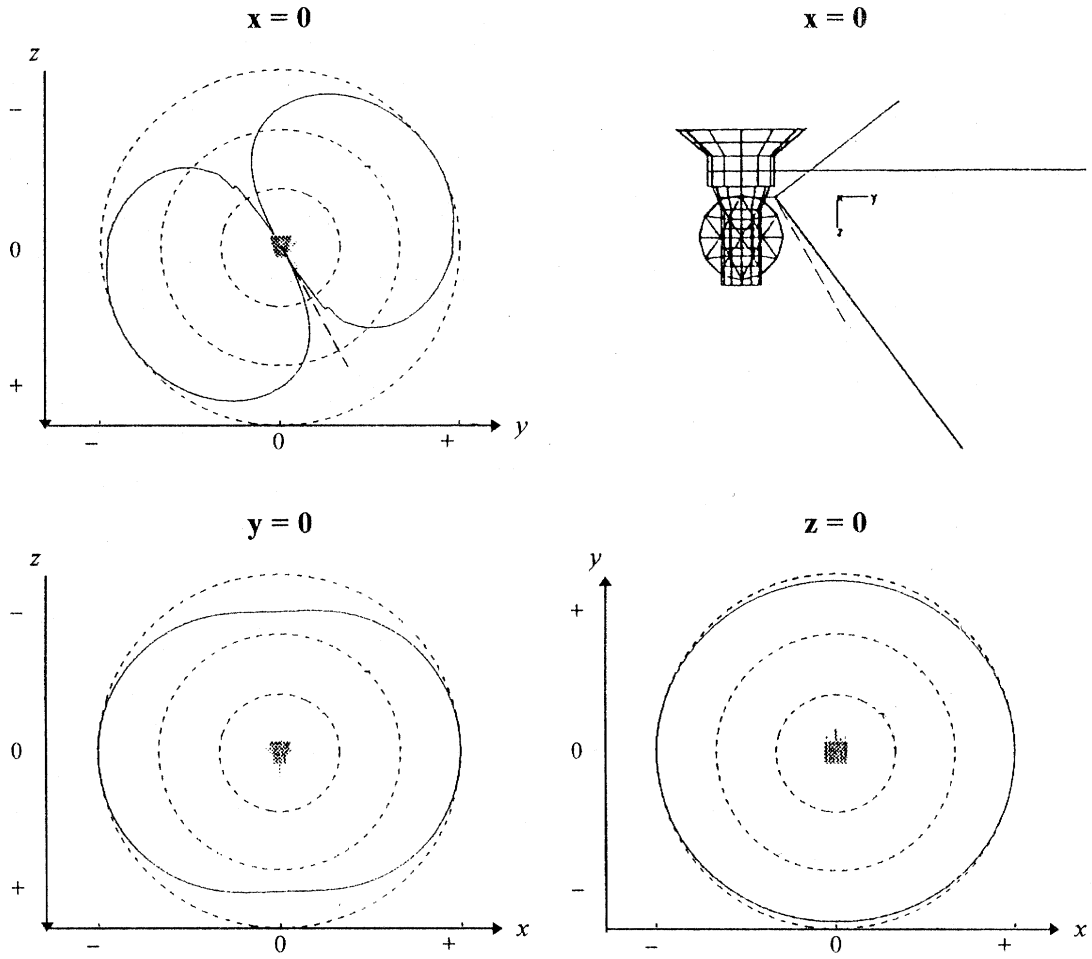

*Figure 5: Radiation patterns of the +**z**-antenna as found by computation using ASAP. The intersections of the 3-dimensional pattern with the main planes of the spacecraft-fixed reference frame are shown. Dashed circles indicate lines of constant radiation power, with a separation of 10 dB. The grid drawing is a projection of the design 2 wire grid, which the pattern is calculated for, onto the yz-plane. The effective length vector of the +**z**-antenna is drawn as dashed straight line in the upper figures.*

3-dimensional wire grid onto the yz-plane. The effective length vector of the +**z**-monopole is drawn in the upper figures for comparison.

4 Discussion

Table 4 again gives the effective length vectors as found from the ASAP calculations for the three monopoles. In addition, the corresponding results determined by rheometry, and the direction of the mechanical antenna elements can be seen. The results from rheometry are determined for the configuration without RTG-shades (therefore slightly differing from the values in Table 2) for maximum coincidence with the ASAP wire grid.

Table 4: Comparison of directions of the mechanical antenna elements and the effective length vectors $\mathbf{h}_{\text{eff}}$ *as obtained by ASAP-computation and rheometry measurements.*

Antenna	Mechanical elements		$\mathbf{h}_{\text{eff}}$ from ASAP		$\mathbf{h}_{\text{eff}}$ from rheometry	
	ϑ	φ	ϑ	φ	ϑ	φ
$+\mathbf{x}$	107.5	24.8	106.5	14.5	107.5	16.3
$-\mathbf{x}$	107.5	155.2	106.5	161.0	107.0	162.9
$+\mathbf{z}$	37.0	90.0	29.0	83.5	31.3	90.3

The values from rheometry are found for the configuration with Huygens probe, but without RTG-shades to provide maximum concurrence with the wire grid used for the ASAP calculations. ϑ and φ are colatitude and azimuth in the spacecraft fixed reference frame, all angular values are given in degrees.

A very good concurrence of the experimental and the computed results can be recognized. Taking into consideration that, apart from deficiencies of the modelling, either method has an inherent inaccuracy of about 2°(in case of rheometry from limits in the precision of the experimental setup and performance, in case of numerical computation from imperfections of algorithm and coding), one sees that the two methods significantly differ only in the effective azimuth φ of the $+\mathbf{z}$-antenna, resulting in two different $\mathbf{h}_{\text{eff}}$ which enclose an angle of about 4°. Even though possible, it is very improbable, that also this difference could stem from the mentioned inaccuracies. The only reasonable origin of this deviation seems to be the different quality of modelling. The wire grid model for the numerical simulations is much more crude than the rheometry model. We already mentioned above the spacecraft features that may have significant influence on the radiation pattern which are still omitted in grid modelling up to now. The values belonging to the $+\mathbf{z}$-antenna in Table 4 verify this supposition. Future simulations with a design 3 grid including these additional features are therefore recommended in order to have the same model basis for the experimental method on the one side and the numerical method on the other side, ensuring that deviations of results do not stem from different qualities of modelling.

The diagram in Figure 6 gives an impression of the quality-dependence on frequency f of high frequency methods and quasistatic methods based on the electrostatic analogy, supposed that the achieved spacecraft modelling quality has the same level in either case. In the low frequency domain the electrostatic analogy methods yield high quality results, whereas high frequency methods work best for wavelengths in the order of the antenna dimension (also getting inappropriate for too high a frequency, $\lambda \ll D$, which is out of our scope). It is crucial that for the frequency range of the Saturn Kilometric Radiation (SKR) all discussed methods are applicable.

In the context of direction finding another method is of great importance, which can be regarded as a special high frequency experimental method (compare Table 1). It is based on the calibration of the antenna system by observing the signals received from known incident electromagnetic waves. This procedure will be applied to the RPWS antennas during the Jupiter flyby utilizing Jovian radio emissions which are well known from the Voyager missions (see Ladreiter et al. [1994, 1995, 1997 (this volume)], Lecacheux [1978], Orthega-Molina and Daigne [1984], Rucker et al. [1996], where further references can

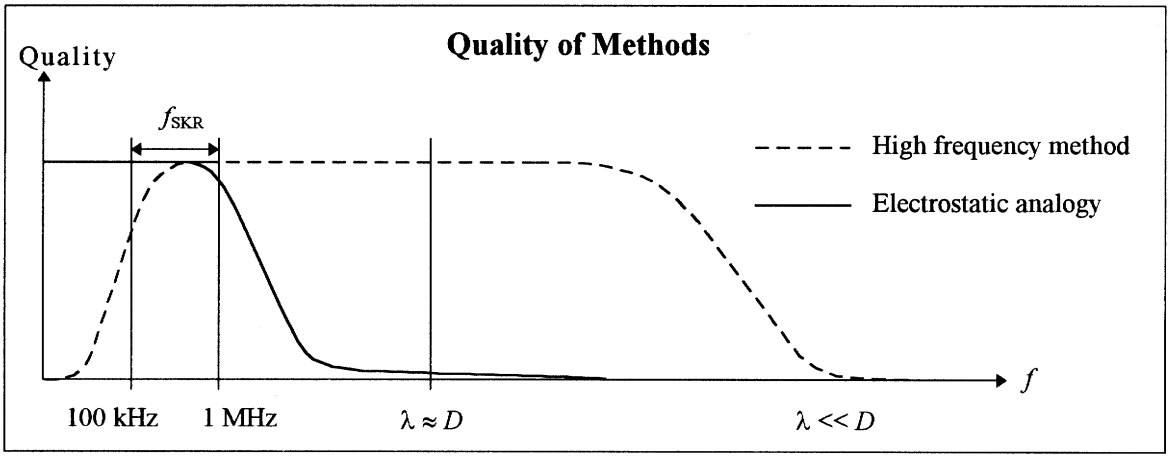

Figure 6: Dependence of the quality of high frequency and electrostatic analogy methods on frequency f. Former are best adapted to problems with wavelenghts λ in the order of the dimension D of the antenna system, whereas latter are appropriate only for $\lambda \gg D$. However, there is a small frequency range, falling into the range f_{SKR} of Saturn Kilometric Radiation, where both methods can be utilized.

be found). As shown by Ladreiter et al. [1995] the numerical calibration is an iterative process which strongly depends on initial values that should not lie too far from the final results. The methods described in this paper are capable of providing good initial values for these future calibrations.